

## Magnetic Resonance Colonography Enables the Efficacy Assessment of Immune Checkpoint Inhibitors in an Orthotopic Colorectal Cancer Mouse Model<sup>1,2</sup>



Yeon Ji Chae<sup>\*,3</sup>, Jinil Kim<sup>\*,3</sup>, Hwon Heo<sup>\*</sup>,  
Chul-Woong Woo<sup>†</sup>, Sang-Tae Kim<sup>†</sup>, Min Jung Kim<sup>‡</sup>,  
Jong Rip Choi<sup>‡</sup>, Dae Hee Kim<sup>‡</sup>, Dong-Cheol Woo<sup>\*,†</sup>,  
Kyung Won Kim<sup>§,3</sup> and Yoonseok Choi<sup>¶,3</sup>

<sup>\*</sup>Department of Convergence Medicine, Asan Medical Center, University of Ulsan College of Medicine, Seoul, Republic of Korea; <sup>†</sup>Convergence Medicine Research Center, Asan Institute for Life Sciences, Asan Medical Center, Seoul, Republic of Korea; <sup>‡</sup>Scripps Korea Antibody Institute, Chuncheon, Gangwon-do, Republic of Korea; <sup>§</sup>Department of Radiology, Asan Medical Center, University of Ulsan College of Medicine, Seoul, Republic of Korea; <sup>¶</sup>Medical Research Institute, Gangneung Asan Hospital, University of Ulsan College of Medicine, Gangneung-si, Gangwon-do, Republic of Korea

### Abstract

Immune checkpoint inhibitors (ICIs) have become an effective therapeutic option for colorectal cancer and studies on these drugs have therefore increased greatly. Efficacy assessments of ICIs in preclinical orthotopic colorectal cancer using MRI have not been reported however due to the difficulties in conducting colorectal imaging. The purpose of this present study was to investigate the feasibility of using magnetic resonance colonography (MRC) to evaluate the efficacy of an ICI, an anti-PD-L1 antibody, in an orthotopic colorectal cancer mouse model. The mouse model was generated by the engraftment of colorectal cancer cells into the submucosal layer of the colon. Anti-cancer efficacy was assessed by tumor volume and metastatic tumor number analyses, and these values were significantly lower in the PD-L1 antibody-treated group compared to the controls. Histological analyses using H&E and Ki-67 immunohistochemical staining confirmed a highly efficacious tumor growth inhibition and enhanced infiltration by CD4+ and CD8+ lymphocytes in the PD-L1 antibody-treated group. We conclude that MRC has the potential to be used for ICI efficacy assessments against orthotopic colorectal cancer mouse model.

*Translational Oncology (2019) 12, 1264–1270*

### Introduction

Immune checkpoint inhibitors (ICIs) have emerged as important next generation anti-cancer therapeutics [1–3] and numerous clinical trials of these agents have yielded promising results [4,5]. ICI trials are being conducted for various subtypes of colorectal cancer (CRC) [6–8]. Pembrolizumab and nivolumab (anti-PD-1 agents) have been approved for high microsatellite instability (MSI-H) [9] or mismatch repair deficiency (dMMR) CRC [10] and several trials on either on anti-PD-L1 antibodies or combinatorial therapies (ICIs and traditional regimens) are currently ongoing [8,11]. Translational studies on ICIs appear to be needed however to establish better treatment strategies for CRC as problems with patient selection and resistance remain [12–14].

Magnetic resonance imaging (MRI) has proved to be an excellent modality for preclinical cancer studies due to its high resolution and

Address all correspondence to: Kyung-Won Kim, M.D., Ph.D., Department of Radiology, Asan Medical Center, University of Ulsan College of Medicine, Seoul, Republic of Korea. or Yoonseok Choi, Ph.D., Medical Research Institute, Gangneung Asan Hospital, University of Ulsan College of Medicine, Gangneung-si, Gangwon-do, Republic of Korea. E-mails: medimash@gmail.com, yschoi21rad@gnah.co.kr

<sup>1</sup> Financial Support: This work was supported by a grant from Basic Science Research Program through the National Research Foundation of Korea (NRF) funded by the Ministry of Education (2016R1D1A1A02937258) and a grant of the Korea Drug Development Fund (KDDF-201606-15), Republic of Korea.

<sup>2</sup> Disclosure and Conflicts of Interest: The authors declare no potential conflicts of interest.

<sup>3</sup> These authors contributed equally to this work.

Received 22 April 2019; Accepted 19 June 2019

© 2019 The Authors. Published by Elsevier Inc. on behalf of Neoplasia Press, Inc. This is an open access article under the CC BY-NC-ND license (<http://creativecommons.org/licenses/by-nc-nd/4.0/>). 1936-5233/19

<https://doi.org/10.1016/j.tranon.2019.06.006>

non-invasiveness [15–17]. For colorectal MR imaging, a bowel enema and colorectal lumen distension are among the preparation steps for image acquisition, a method that is collectively termed magnetic resonance colonography (MRC) [18–20]. As with clinical studies, these techniques have been adapted for preclinical colorectal MR imaging. Following the pioneering studies of Boraschi et al., and Hensley et al., several subsequent reports have described the successful MRC imaging of rodent colorectal regions [21–24]. Furthermore, several studies adapted the functional imaging techniques to visualize the mouse colorectal regions with MRI [25–28]. However, no study to date has assessed ICI efficacy using the MRC method despite the importance of using a syngeneic and orthotopic mouse model for such an evaluation [29–31].

In this present study, we assessed the feasibility of MRC as an ICI efficacy evaluation tool in an orthotopic CRC mouse model.

## Materials and Methods

### Cells

Mouse colon cancer cells (MC38) and human cancer cell lines (SKOV3, MDA-MB-231, MCF-7, H460, PC3) were purchased from the Korean Cell Line Bank (KCLB, Seoul, Korea). All cells were cultured in Dulbecco's modified Eagle's medium (DMEM, GIBCO, Thermo Fisher Scientific, Waltham, MA) supplemented with 10% (v/v) heat-inactivated fetal bovine serum (FBS; GIBCO) at 37 °C in a 5% CO<sub>2</sub> humidified environment.

### Anti-PD-L1 Antibody

A monoclonal anti-PD-L1 antibody (PD-L1 mAb; PL110) was developed using phage display antibody screening as an immunoncology therapeutic candidate and showed strong inhibitory effects on the PD-1/PD-L1 interaction *in vitro* and *in vivo* (ref. to be described later after the English proofreading) [32]. Full IgG1 constructs were generated by PCR amplification of the VH, VL domains from an scFv-expressing vector and subcloning of these amplicons into the heavy chain and light chain expression vectors, pCEP4-VH and pCEP4-VL respectively. These two vectors were purified using a DNA Maxi-prep kit from Qiagen and transfected into HEK293F cells at a 1:2 DNA ratio (heavy chain: light chain) using FectoPRO transfection reagent (Polypplus transfection; Thermo Fisher Scientific) in accordance with the manufacturer's instructions. After 10 days of antibody production in 'FreeStyle 293' expression medium (Invitrogen, Thermo Fisher Scientific), supernatant containing the antibodies was harvested and purified using open-column chromatography with protein A resin (GenScript; Thermo Fisher Scientific). Antibodies were eluted with 50 mM citric acid, and then rapidly neutralized with 1 M Tris-HCl pH 9.0 and dialyzed with PBS. A control anti-PD-L1 antibody, 'MPDL' was obtained using the same vectors. Expression and purification systems in which the VH and VL sequences were derived from Roche's 'Atezolizumab' sequences and their cDNAs were chemically synthesized (Macrogen, Seoul, Korea).

### Flow Cytometry

MC38 cells were stimulated in the absence or presence of 100 ng/ml mouse IFN- $\gamma$  (Cat#315-05, PeproTech, Rocky Hill, NJ) for 18 hours. Cells were then harvested and resuspended in FACS buffer (2% BSA, 0.02% Na<sub>3</sub>N in PBS), and stained with 10  $\mu$ g/ml MPDL3280A or PL110 for 30 minutes at 4 °C. Cells were washed with FACS buffer and incubated for 30 minutes at 4 °C with Alexa Fluor 488-labeled goat anti-human IgG H&L (Jackson ImmunoR-

search Laboratories Inc., West Grove, PA). Various human tumor cells were harvested and resuspended in FACS buffer and stained with 10  $\mu$ g/ml PL110 for 30 minutes at 4 °C. Cells were then washed with FACS buffer and incubated for 30 minutes at 4 °C with Alexa Fluor 488-labeled goat anti-human IgG H&L (Jackson ImmunoResearch Laboratories Inc.). Flow cytometry data were acquired on a FACS Calibur flow cytometer (BD) and analyzed using FlowJo software.

### Ethics on Animal Experiments

C57BL/6 (8 weeks old, male) were purchased from Orient Animal Laboratory (Seoul, South Korea). All animal experiments were performed in accordance with the guidelines of the National Institutes of Health and the recommendations of the committee on animal research at our institution. The animal protocols were approved by the Committee on the Ethics of Animal Experiments at Asan Medical Center (IACUC No. 2018–12-240).

### Fluorescence Labeling and Optical Imaging

The PL110 anti-PD-L1 antibody was labeled using an Alexa Fluor 647 Antibody Labelling Kit (Thermo Fisher Scientific, Waltham, MA). The collected labeled antibodies were stabilized at room temperature for 1 hour. Following this, non-labeled control PL110, Alexa Fluor-labeled 647-PL110 (2 mg/kg), and Alexa Fluor-labeled 647-PL110 (10 mg/kg) were separately injected intravenously into mice bearing MC38 tumors (C57BL/6 mouse model subcutaneously injected with 1 x 10<sup>6</sup> MC38 cells, n = 4 per group). Serial fluorescence images were acquired using IVIS Lumina II (PerkinElmer, Waltham, MA). Parameters for image acquisition were as follows: exposure time, 1 s; and f/stop, 1. The peak total signal was measured using Living Image 4.2 software (Caliper Life Sciences, Hopkinton, MA) using regions of interest (ROIs) at the tumors that reflected the accumulated amount of Alexa Fluor 647 labeled PL110.

### Orthotopic Colorectal Tumor Mouse Model and PL110 Administration

All orthotopic mouse models were generated by injection of 1 x 10<sup>5</sup> MC38 cells into these animals near to the distal regions of the colon and adjacent to the area right above the rectum. Tumor bearing mice were randomly divided into untreated, PL110 2 mg/kg treated and PL110 10 mg/kg treated groups (n = 10 for each group; hereafter referred to as control, PL110-2 mg, and PL110-10 mg, respectively). Antibodies were dissolved in saline (0.1 ml) and injected intraperitoneally. PL110 or saline was first administered at 1 week after tumor cell engraftment, when the tumor had reached approximately 5–6 mm in diameter and 70 to 130 mm<sup>3</sup> in volume, and three more times of injection were followed by 3 days of interval from the beginning day of PL110 administration. Mice were euthanized at 21 days after tumor cell engraftment (Supplementary Figure 1).

### Magnetic Resonance Colonography and Tumor Volume Measurement

MRC was used to monitor the orthotopic colorectal tumors and their metastatic foci in the mouse model. A cleansing enema was first performed using 150  $\mu$ l of saline. The colorectum was then subsequently filled with Fluorinert as it produces no MR proton signal. T1-weighted images (T1w) with fat suppression were acquired in surviving mice using a 9.4 T MRI scanner (Agilent, Inc.) prior to and at 7, 14 and 21 days after tumor cell engraftment. The MR parameters for the T1w coronal images were as follows: TR/TE,

1000/8.99 ms; FOV, 50×40 mm; matrix, 192×128; slice, 12; and a slice thickness of 1 mm. The volumes of the orthotopic colorectal tumors were calculated by multiplying the summed tumor areas by the slice thickness.

**Metastatic Tumor Quantification**

The number of metastatic tumor foci was counted on MR images and by visual inspection. For the quantification of these foci by MRI, T1w axial images were obtained after the scanning of MRC coronal images with the following parameters: TR/TE, 1100/9.15 ms; FOV, 25×40 mm; matrix, 128×192; slice, 24; and a slice thickness of 2 mm. The metastatic foci were counted on every T1w axial image of the tumor engrafted mice by two trained individuals. Visual inspection of the gross histologic specimens was carried out after the mice were euthanized.

**Histological Analyses**

For histological analyses, hematoxylin and eosin (H&E) staining and immunohistochemistry (IHC) were performed using primary and metastatic tumor specimens. Anti-Ki67 antibody (ab15580, Abcam, Cambridge, UK) was used with a goat anti-rabbit IgG-HRP secondary antibody (sc-2030; Santa Cruz Biotechnology, Dallas, TX, USA). H&E and Ki67 stained images were obtained under a Zeiss AxioscopeII microscope (Carl Zeiss, Oberkochen, Germany). IHC signals were quantified using ImageJ software (National Institutes of Health, Bethesda, MD, U.S.A.). Anti-CD3 (ab5690, Abcam, Cambridge, UK), anti-CD4 (sc-13,573, Santa Cruz Biotechnology) and anti-CD8 (sc-7970, Santa Cruz Biotechnology) antibodies were

used with an Alexa Fluor 647-labeled goat anti-rabbit IgG H&L (A21244, Thermo Fisher Scientific), Alexa Fluor 594-labeled goat anti-rat IgG H&L (A11007, Thermo Fisher Scientific) and Alexa Fluor 488-labeled goat anti-mouse IgG H&L (A10680, Thermo Fisher Scientific) secondary antibodies, respectively. Fluorescent images were obtained with a Zeiss 780 confocal microscope (Carl Zeiss).

**Statistical Analyses**

Statistical analyses were conducted using SPSS version 20.0 software (SPSS, Chicago, IL). Differences in the tumor volume growth between groups were analyzed by repeated measures ANOVA (RM-ANOVA), followed by a Tukey's HSD post-hoc test. Kaplan–Meier curves according to Breslow (generalized Wilcoxon) were used to estimate survival. One-way ANOVA with the Tukey's HSD post-hoc test was performed to compare the mean values between the study groups and a *P*-value <.05 was considered statistically significant.

**Results**

**Validation of PL110 Targeting by Flow Cytometry and Optical Imaging**

We evaluated the targeting ability of PL110 against the PD-L1 antigen by flow cytometry. Alexa Fluor 488-labeled PL110 showed a good binding affinity to MC38 cells in the presence or absence of IFN- $\gamma$  stimulation. Although this binding was not as robust as the MPDL, strong 488 signals were observed in PL110-treated MC38 cells compared to a naïve antibody labeled with Alexa Fluor 488 (Figure 1A). In addition, we incubated PL110 with several human

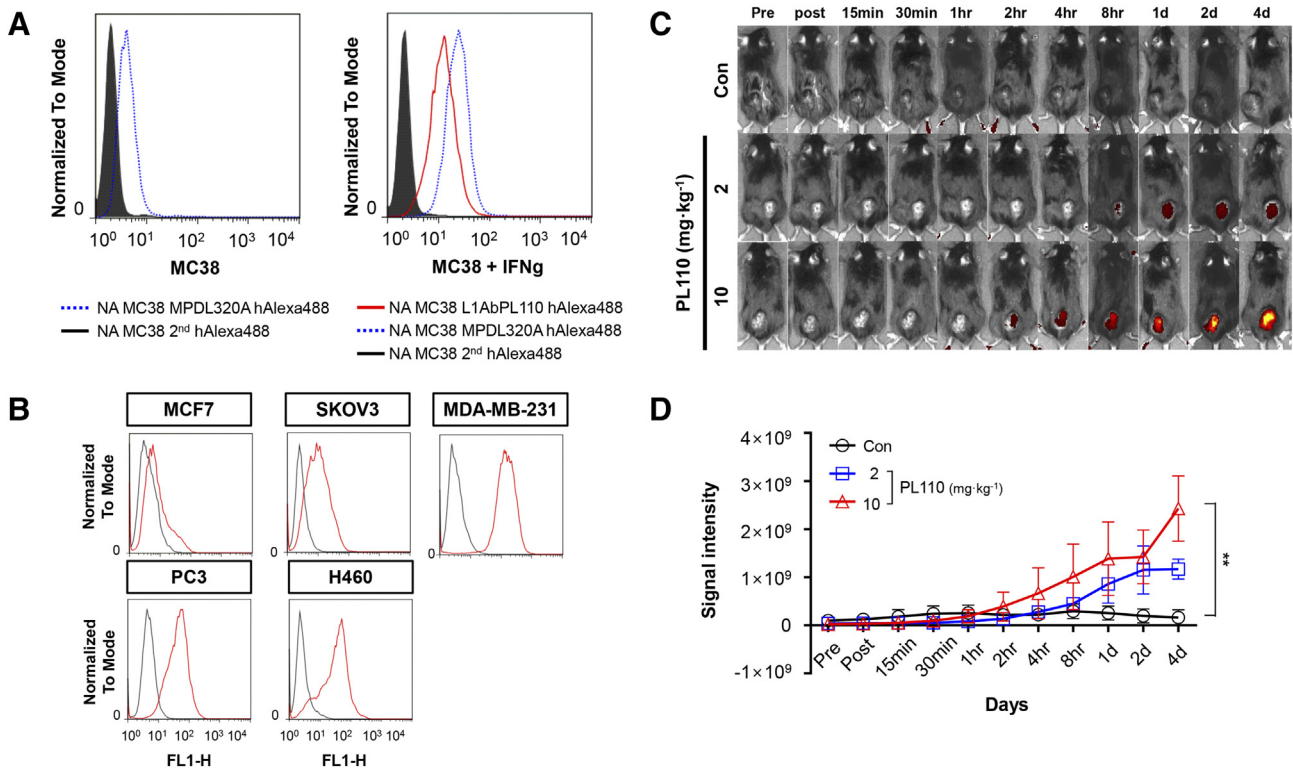


**Figure 1.** Validation of the PD-L1 targeting abilities of PL110 in cell lines and in implanted tumors. (A) FACS analysis showing the binding of Alexa Fluor 488-labeled PL110 to IFN- $\gamma$  (100 ng/ml) stimulated MC38 tumor cells. (B) Alexa Fluor 488-labeled PL110 binding to PD-L1 expressing human cell lines (MDA-MB-231, H460, PC3). (C) Serial fluorescence images showing the accumulation of Alexa Fluor 488-labeled PL110 (2 mg/kg or 10 mg/kg) at MC38-implanted tumor sites at 2 hours after injection. \**P* < .05, \*\**P* < .01.

cancer cell lines for the further evaluation of its binding capability. Compared to MCF-7 and SKOV3 cells that are known to express low or moderate levels of PD-L1 [33], ample Alexa Fluor 488 signals were observed in the MDA-MB-231, H460 and PC3 cell lines that were incubated with PL110 antibody labeled with Alexa Fluor 488 (Figure 1B). In the in vivo assessments, we injected Alexa Fluor 647-labeled PL110 at different concentrations (2 mg/kg or 10 mg/kg) into the subcutaneously implanted MC38 tumor model. A focal signal appeared at the MC38 tumor implantation site after 2 hours in the Alexa Fluor 647-labeled PL110 10 mg/kg group. At 4 days after injection, both the Alexa Fluor 647-labeled PL110 2 mg/kg and Alexa Fluor 647-labeled PL110 10 mg/kg injected groups showed fluorescence accumulation, but not the control mice. The signal intensity was most significant in the 10 mg/kg injected animals compared to the controls ( $P = .007$ ). These results confirmed that PL110 can target PD-L1 expressing tumors (Figure 1C).

### Therapeutic Efficacy Assessment of PL110 in the Colorectal Cancer Mouse Model Using MRC

All the MRC images for the experimental mice revealed excellent distension of the colorectal lumen following Fluorinert insertion and enabled monitoring of the tumors in the colorectal lumen. To monitor the anti-cancer effects of PL110 on tumor growth in the mice, coronal MR images were obtained prior to and at 7, 14, and 21 days after tumor cell engraftment (Figure 2A). Both PL110-injected groups showed a significant decrease in tumor volumes compared to the control group (2 mg,  $P = .044$ ; 10 mg  $P = .001$ ). However, no significant difference was observed between the PL110-2 mg and PL110-10 mg mice (Figure 2B). To investigate whether metastatic tumor foci could be monitored and quantified by MRC, axial MR images were obtained (Figure 2C). The numbers of metastatic tumors were analyzed on day 21 and were significantly decreased in the PL110-10 mg animals on MRI ( $2.13 \pm 0.83$ ) compared to the

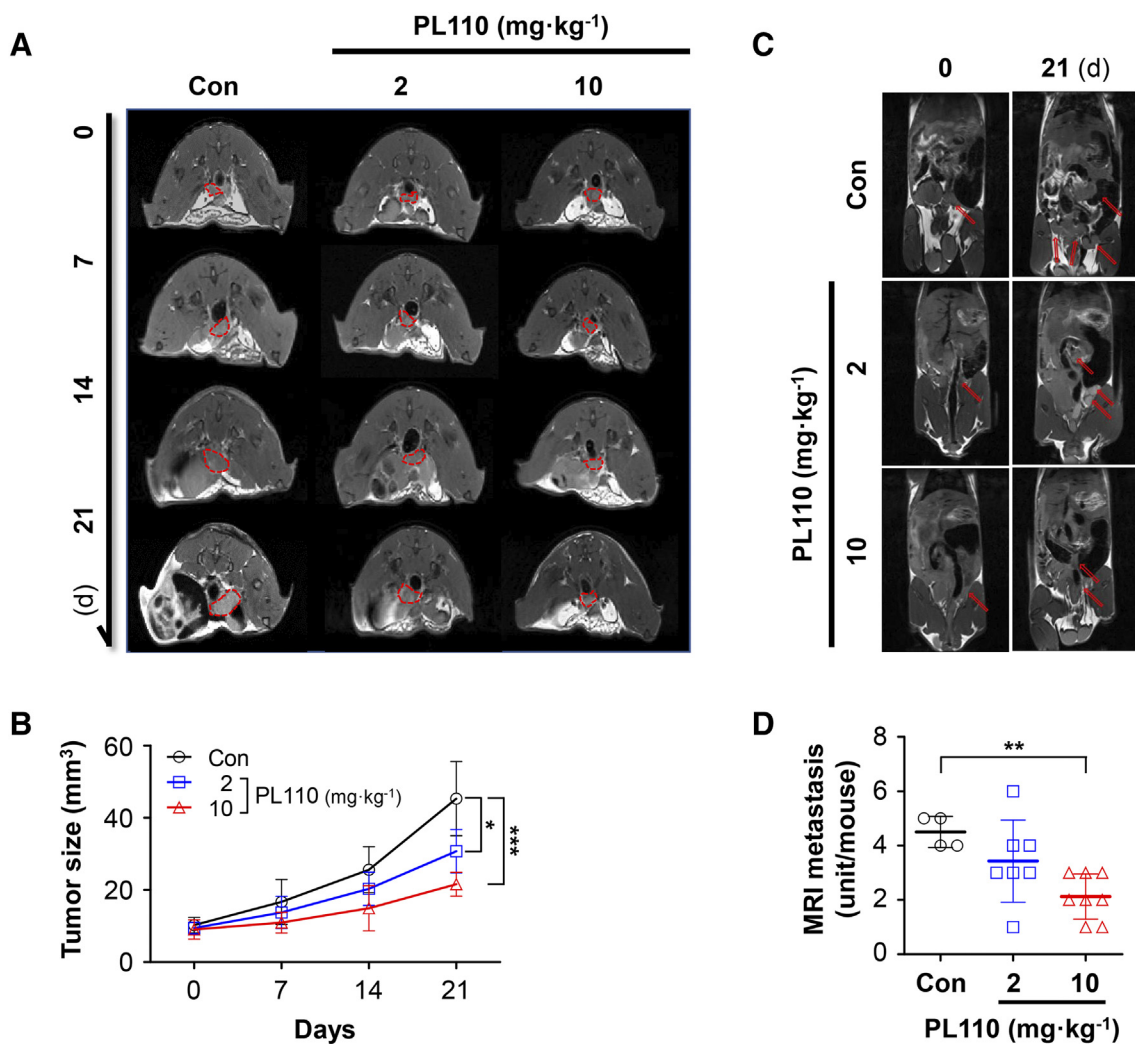


**Figure 2.** Analysis of tumor growth and metastatic tumor quantification using MRC. (A) Coronal MR images of primary tumor growth were monitored longitudinally on days 0, 7, 14 and 21. (B) Tumor volume analysis by MRC revealed anti-cancer effects in both the PL110-2 mg and PL110-10 mg groups compared to the control group. Data represent the mean  $\pm$  standard deviation (SD);  $*P < .05$ ,  $***P < .001$ . (C) Axial MR images were obtained for metastatic tumor quantification on day 21. (D) Compared to the controls, the PL110-10 mg mice showed significantly fewer metastases. No significant differences were evident between the PL110-2 mg and control groups although slightly lower numbers were observed in the PL110-2 mg mice;  $**P < .01$ . The red arrows indicate the primary and metastatic tumor foci.

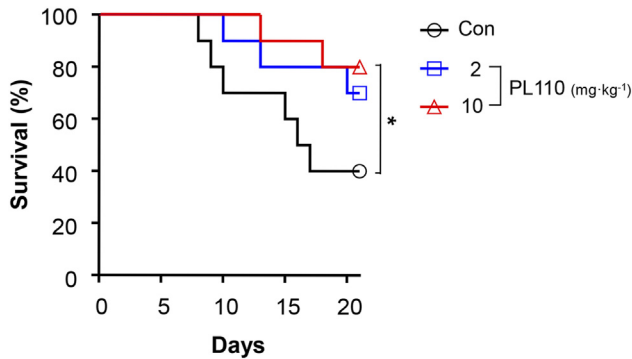


**Figure 3.** Kaplan–Meier survival curve analysis. Survival analysis of the control, PL110-2 mg, and PL110-10 mg groups showing a significant improvement in the PL110-10 mg animals compared to the control group; (n = 10/group), \**P* < .05.

controls ( $4.5 \pm 0.58$ , *P* = .008). However, no significant differences in these foci numbers were observed between control vs. PL110-2 mg and between PL110-2 mg vs. PL110-10 mg mice (Figure 2D). We also counted the metastatic foci by visual inspection on the day of euthanization and found a significant decrease in the PL110-10 mg mice compared to the controls ( $3.25 \pm 0.50$  vs.  $1.63 \pm 0.52$ , *P* = .031). No significant differences were observed however between the control vs. PL110-2 mg and PL110-2 mg vs. PL110-10 mg animals (Supplementary Figure 2A). The quantified data from the MR images and visual inspections showed a positive correlation (*R* = 0.8569, *P* < .001; Supplementary Figure 2B). Finally, the overall survival rates of the treatment and control groups were analyzed. The survival

rate of the PL110-10 mg mice (80%, *P* = .047) was significantly higher than the controls (30%), however significant differences were not found between the PL110-2 mg animals and control animals though higher survival rate was observed than the controls as was that of the PL110-10 mg animal (70%, *P* = .047). The survival rates between the PL110-2 mg and PL110-10 mg mice also showed no significant differences (Figure 3).

**Histological Analyses of Tumor Cell Proliferation and Lymphocyte Infiltration after PL110 Administration**

Tumor tissues from the mouse model were H&E-stained for the preliminary examination of the tumor status. All primary tumors were found in the submucosal layers. The proliferation tendencies of primary and metastatic tumor cells and degree of lymphocyte infiltration were investigated. Compared to the control group, the PL110 treated groups showed reduced tumor volumes and greater infiltration of lymphocytes inside the tumors (Figure 4A). We quantified the proliferation tendencies of the tumors by calculating the Ki-67-positive cell percentages of the primary tumor and metastatic foci in each individual mouse. In the analyses of the primary tumors, significantly lower values were observed in the PL110-2 mg ( $27.33 \pm 5.55$ ) and the PL110-10 mg ( $17.81 \pm 1.35$ ) groups compared to the controls ( $80.11 \pm 4.35$ , *P* < .001, *P* < .001). In the metastatic tumors, lower Ki-67 expression was observed in PL110-10 mg ( $36.45 \pm 4.60$ ) animals compared to the controls ( $66.11 \pm 3.22$ , *P* = .023) but no statistically significant differences in Ki-67 expression were observed between the control vs. PL110-2 mg and PL110-2 mg vs. PL110-10 mg groups (Figure 4B).

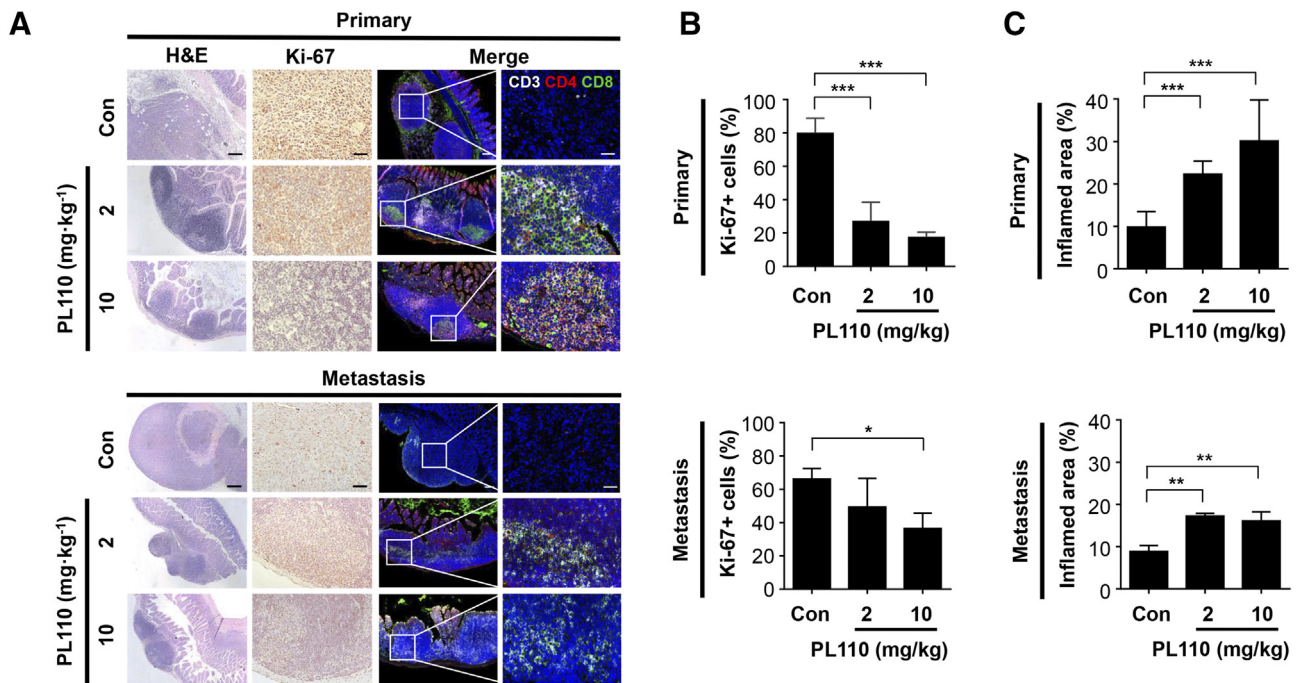


**Figure 4.** Histological analyses on tumor proliferation and T-cell infiltrated regions. (A) H&E staining, Ki67 expression analysis and, triple immunofluorescence staining of CD3, CD4 and CD8 was performed to analyze the tumor proliferation and T-cell infiltration. Original magnification  $\times 50$ . (B) Ki-67-positive percentages were significantly lower in the PL110-2 mg and PL110-10 mg mice at the primary tumor sites. Significant differences in these percentages were also observed for the metastatic foci. Original magnification  $\times 200$  (C) Inflamed area analyses showing that T-cell infiltration was significantly higher in the PL110-10 mg group at both the primary and metastatic tumor sites; \**P* < .05, \*\**P* < .01, \*\*\**P* < .001. Nuclear staining: blue, CD3; white, CD4; red, CD8; green. Original magnification  $\times 50$  and  $\times 200$ .

We evaluated the degree of T-cell infiltration by immunofluorescence staining. Cytotoxic T-cell (CD3 + CD8+) and helper T-cell (CD3 + CD4+) recruitment to tumor regions (inflamed areas) was increased in the PL110 treated groups. In the case of primary tumors, cold tumors (T-cell exclusion) were observed in the control mice whereas hot tumors (inflamed) were observed in the PL110-2 mg and the PL110-10 mg animals. Inflamed areas were also significantly increased in the PL110-2 mg (22%) and PL110-10 mg (30%) mice compared to the controls (10%,  $P < .001$ ,  $P < .001$ ). The cytotoxic T-cell (CD3 + CD8+) and helper T-cell (CD3 + CD4+) inflamed areas in the case of metastatic tumors were significantly increased in the PL110 treated groups (PL110-2 mg: 17%, PL110-10 mg: 16%) compared to the controls (9%,  $P = .002$ ,  $P = .003$ ). However, there were no statistically significant differences in this regard between the control vs. PL110-2 mg and PL110-2 mg vs. PL110-10 mg groups for either the primary tumor or metastatic tumors (Figure 4C).

## Discussion

The results of our present study using an orthotopic colorectal cancer model suggest that MRC may be a viable assessment tool for the anti-cancer efficacy of ICIs. MRC enabled the noninvasive monitoring of tumor growth at the sites of engraftment in these mice along the experimental periods. Monitoring of the tumor inhibition effects after the administration of PL110 was readily achieved because the bowel enema and Fluorinert insertion produced good image quality. In addition, metastatic foci observations were possible because they could be counted using the MR images even though small discrepancies existed with the counts from a visual inspection. The total numbers of metastatic foci on the MR images were less than those determined by visual inspection which may have been due to the detection threshold for small tumors on an MRI (2D: ~1.0 mm, 3D: ~1.0mm<sup>3</sup> in approximation) [22,26]. Notably however, the detection of anti-metastatic effects by MRI and visual inspection was consistent and a positive correlation was observed between the numbers of metastatic tumor foci determined by MRI and through visual inspection. With regard to sensitivity limits, other imaging modalities such as PET/CT and PET/MRI would be a better choice for metastatic colorectal cancer monitoring. However, due to the convenience of using a radioisotope-free method and the cost of imaging, MRC remains a good modality for ICI efficacy assessments in metastatic tumor analysis.

Our histological analyses of the model mice supported the anti-cancer effects of PL110 that were observed on the follow-up MR images. Proliferation marker (Ki-67) staining analyses and inflamed area analyses using lymphocyte marker (CD3, CD4, and CD8) staining provided further evidence of these anti-cancer effects of PL110 in the CRC mouse model. Moreover, as we had confirmed that PL110 can effectively target PD-L1 expressing cell lines and the primary tumors, we can conclude that the anti-cancer effects of PL110 are related to the immune cell responses to an immune-checkpoint PD-L1 blockade.

In conclusion, MRC shows good utility as an ICI efficacy assessment tool in an orthotopic colorectal cancer model. Future studies of combinatorial therapies involving ICIs and traditional cancer regimens on the orthotopic colorectal cancer model will be available with this technique. Since the generation of orthotopic models and longitudinal monitoring of internally growing tumors will be important in assessing the efficacy of ICIs against colorectal cancer,

we anticipate that MRC will prove useful for the efficacy assessment of newly developed ICIs.

Supplementary data to this article can be found online at <https://doi.org/10.1016/j.tranon.2019.06.006>.

## Acknowledgements

This work was supported by a grant from Basic Science Research Program through the National Research Foundation of Korea (NRF) funded by the Ministry of Education (2016R1D1A1A02937258) and a grant of the Korea Drug Development Fund (KDDF-201606-15), Republic of Korea.

## References

- [1] Couzin-Frankel J (2013). Breakthrough of the year 2013. Cancer immunotherapy. *Science* **342**, 1432–1433.
- [2] Koster BD, de Gruijl TD, and van den Eertwegh AJ (2015). Recent developments and future challenges in immune checkpoint inhibitory cancer treatment. *Curr Opin Oncol* **27**, 482–488.
- [3] Lee L, Gupta M, and Sahasranaman S (2016). Immune Checkpoint inhibitors: An introduction to the next-generation cancer immunotherapy. *J Clin Pharmacol* **56**, 157–169.
- [4] Zavala VA and Kaleris AM (2015). New clinical advances in immunotherapy for the treatment of solid tumours. *Immunology* **145**, 182–201.
- [5] Darvin P, Toor SM, Sasidharan Nair V, and Elkord E (2018). Immune checkpoint inhibitors: recent progress and potential biomarkers. *Exp Mol Med* **50**, 165.
- [6] Le DT, Uram JN, Wang H, Bartlett BR, Kemberling H, Eyring AD, Skora AD, Lubner BS, Azad NS, and Laheru D, et al (2015). PD-1 Blockade in Tumors with Mismatch-Repair Deficiency. *N Engl J Med* **372**, 2509–2520.
- [7] Overman MJ, McDermott R, Leach JL, Lonardi S, Lenz HJ, Morse MA, Desai J, Hill A, Axelson M, and Moss RA, et al (2017). Nivolumab in patients with metastatic DNA mismatch repair-deficient or microsatellite instability-high colorectal cancer (CheckMate 142): an open-label, multicentre, phase 2 study. *Lancet Oncol* **18**, 1182–1191.
- [8] Lynch D and Murphy A (2016). The emerging role of immunotherapy in colorectal cancer. *Ann Transl Med* **4**, 305.
- [9] Administration UfaD (2017). *FDA grants accelerated approval to pembrolizumab for first tissue/site agnostic indication*, Vol. Editor (ed)^(eds). US Food and Drug Administration: City; 2017 2017.
- [10] Administration UfaD (2017). *FDA grants nivolumab accelerated approval for MSI-H or dMMR colorectal cancer*, Vol. Editor (ed)^(eds). US Food and Drug Administration: City; 2017 2017.
- [11] Tapia Rico G and Price TJ (2018). Atezolizumab for the treatment of colorectal cancer: the latest evidence and clinical potential. *Expert Opin Biol Ther* **18**, 449–457.
- [12] Syn NL, Teng MWL, Mok TSK, and Soo RA (2017). De-novo and acquired resistance to immune checkpoint targeting. *Lancet Oncol* **18**, e731–e741.
- [13] Dijkstra KK, Voabil P, Schumacher TN, and Voest EE (2016). Genomics- and Transcriptomics-Based Patient Selection for Cancer Treatment With Immune Checkpoint Inhibitors: A Review. *JAMA Oncol* **2**, 1490–1495.
- [14] Havel JJ, Chowell D, and Chan TA (2019). The evolving landscape of biomarkers for checkpoint inhibitor immunotherapy. *Nat Rev Cancer* **19**, 133–150.
- [15] O'Farrell AC, Shnyder SD, Marston G, Coletta PL, and Gill JH (2013). Non-invasive molecular imaging for preclinical cancer therapeutic development. *Br J Pharmacol* **169**, 719–735.
- [16] Lyons SK (2015). Imaging Mouse Models of Cancer. *Cancer J* **21**, 152–164.
- [17] Wang Y, Tseng JC, Sun Y, Beck AH, and Kung AL (2015). Noninvasive imaging of tumor burden and molecular pathways in mouse models of cancer. *Cold Spring Harb Protoc* **2015**, 135–144.
- [18] Luboldt W, Steiner P, Bauerfeind P, Pelkonen P, and Debatin JF (1998). Detection of mass lesions with MR colonography: preliminary report. *Radiology* **207**, 59–65.
- [19] Zijta FM, Bipat S, and Stoker J (2010). Magnetic resonance (MR) colonography in the detection of colorectal lesions: a systematic review of prospective studies. *Eur Radiol* **20**, 1031–1046.

- [20] Lauenstein TC, Kuehle CA, and Ajaj W (2005). MR imaging of the large bowel. *Magn Reson Imaging Clin N Am* **13**, 349–358 vii.
- [21] Boraschi P, Neri E, Vannucci L, Vagli P, Braccini G, and Bartolozzi C (2003). Double-contrast MR colonography: in vivo experimental study in an animal model. *Med Sci Monit* **9**, BR363–.
- [22] Hensley HH, Chang WC, and Clapper ML (2004). Detection and volume determination of colonic tumors in Min mice by magnetic resonance micro-imaging. *Magn Reson Med* **52**, 524–529.
- [23] Young MR, Ileva LV, Bernardo M, Riffle LA, Jones YL, Kim YS, Colburn NH, and Choyke PL (2009). Monitoring of tumor promotion and progression in a mouse model of inflammation-induced colon cancer with magnetic resonance colonography. *Neoplasia* **11**, 237–246 231p following 246.
- [24] Ileva LV, Bernardo M, Young MR, Riffle LA, Tatum JL, Kalen JD, and Choyke PL (2014). In vivo MRI virtual colonography in a mouse model of colon cancer. *Nat Protoc* **9**, 2682–2692.
- [25] Zhang Z, Li W, Blatner NR, Dennis KL, Procissi D, Khazaie K, and Larson AC (2013). Quantitative magnetic resonance imaging in the transgenic APC (Delta468) mouse model of hereditary colon cancer. *Mol Imaging* **12**, 59–66.
- [26] Quarles CC, Lepage M, Gorden DL, Fingleton B, Yankeelov TE, Price RR, Matrisian LM, Gore JC, and McIntyre JO (2008). Functional colonography of Min mice using dark lumen dynamic contrast-enhanced MRI. *Magn Reson Med* **60**, 718–726.
- [27] Mustafi D, Fan X, Dougherty U, Bissonnette M, Karczmar GS, Oto A, Hart J, Markiewicz E, and Zamora M (2010). High-resolution magnetic resonance colonography and dynamic contrast-enhanced magnetic resonance imaging in a murine model of colitis. *Magn Reson Med* **63**, 922–929.
- [28] Biton IE, Stettner N, Brener O, Erez A, Harmelin A, and Garbow JR (2018). Assessing Mucosal Inflammation in a DSS-Induced Colitis Mouse Model by MR Colonography. *Tomography* **4**, 4–13.
- [29] Gura T (1997). Systems for identifying new drugs are often faulty. *Science* **278**, 1041–1042.
- [30] Budhu S, Wolchok J, and Merghoub T (2014). The importance of animal models in tumor immunity and immunotherapy. *Curr Opin Genet Dev* **24**, 46–51.
- [31] Mittal VK, Bhullar JS, and Jayant K (2015). Animal models of human colorectal cancer: Current status, uses and limitations. *World J Gastroenterol* **21**, 11854–11861.
- [32] Kim DH, Lee ES, Kim MJ, Tae N, and Choi JR (2019). Antibodies against programmed death-ligand 1 and uses thereof, PCT/KR2019/004373 filed April 11; 2019 .
- [33] Grenga I, Donahue RN, Lepone L, Bame J, Schlom J, and Farsaci BJJfloC (2014). PD-L1 and MHC-I expression in 19 human tumor cell lines and modulation by interferon-gamma treatment, **2**; 2014 P102.